Available online at www.sciencedirect.com
SCIENCE DIRECT®
Journal of Power Sources 145 (2005) 133–138
JOURNAL OF POWER SOURCES
www.elsevier.com/locate/jpowsour

Imaging of CH_4 decomposition around the Ni/YSZ interfaces under anodic polarization

Teruhisa Horita *, Katsuhiko Yamaji, Tohru Kato, Haruo Kishimoto, Yueping Xiong, Natsuko Sakai, Manuel E. Brito, Harumi Yokokawa

National Institute of Advanced Industrial Science and Technology (AIST), AIST Central 5, Higashi 1-1-1, Tsukuba, Ibaraki 305-8565, Japan

Accepted 21 December 2004
Available online 26 April 2005

Abstract

The catalytic activities of Ni-mesh/YSZ samples for CH_4 decomposition and reaction with reformed gases were compared under voltage-applied condition (fuel cell operation condition) by imaging analysis of labeled gases with secondary ion mass spectrometry (SIMS). The effect of applied voltages was compared in the mixture of CH_4, D_2O, and $^{18}O_2$ to label the movements of hydrogen and oxygen. A significant carbon deposition was observed at the Ni-mesh under zero-voltage condition. However, the applied voltage formed a thin oxide layer on the Ni surface and eliminated the deposited carbon on the Ni surface. Oxygen spill-over around the Ni/YSZ interfaces could effectively eliminate the deposited carbon. A possible reaction mechanism was considered for the optimum metal–oxide interfaces of SOFCs.

Keywords: SOFC; Imaging; Secondary ion mass spectrometry (SIMS); Isotope labeling; Ni/YSZ interface

1. Introduction

Because of their high operation temperature (1073–1273 K), solid oxide fuel cells (SOFCs) can utilize hydrocarbons with internal reforming. Steam reforming is one of the promising methods to utilize hydrocarbons in SOFCs as follows:

$$CH_4 + H_2O = CO + 3H_2 \quad (1)$$

$$CO + H_2O = CO_2 + H_2 \quad (2)$$

where Eqs. (1) and (2) are called the steam reforming and shift reactions, respectively. At 1273 K, the steam reforming reaction and shift reaction proceed very fast, and relatively high performances have been reported in SOFC stacks. When the operation temperature of SOFCs is reduced to lower than 1073 K, the steam/carbon ratio should be high enough (more than 2) to prevent carbon deposition. On the other hand, the amounts of steam should be as small as possible in terms of the efficiency of the SOFC systems. Therefore, minimum steam partial pressure and electrochemical oxidation of CH_4 must be considered in the following equation:

$$CH_4 + 4O^{2-} = CO_2 + 2H_2O + 8e^- \quad (3)$$

where O^{2-} is conducted oxide ions through the electrolyte from cathode to anode. Eq. (3) does not normally proceed quickly with Ni/YSZ anodes and a number of papers have been written on this (for example, see reference [1]). In order to realize a SOFC system with internal steam reforming at lower than 1073 K, it is desirable to optimize the electrode/electrolyte interface materials and structures. In recent years, several authors reported active metal–oxide combinations, such as Ni–CeO_2 based oxide and Cu–CeO_2 based oxide [2–5]. However, a porous metal–oxide mixture (that is called "cermet") was difficult in determining the effect factors for CH_4 decomposition and electrochemical oxidation. The effective factors for the electrochemical reaction of CH_4 have not been clarified yet.

* Corresponding author. Tel.: +81 29 861 4542/4540; fax: +81 29 861 4542/4540.
E-mail address: t.horita@aist.go.jp (T. Horita).

0378-7753/$ – see front matter © 2005 Elsevier B.V. All rights reserved.
doi:10.1016/j.jpowsour.2004.12.075

The present study aims to clarify the role of metal and oxide on the decomposition and steam reforming of CH_4 under low steam partial pressures. We have reported the effect of oxides [6] and metals [7] on the decomposition and/or steam reforming of CH_4 by isotope labeling/secondary ion mass spectrometry (SIMS) imaging analyses. The active parts for carbon deposition and reaction with light elements are clearly imaged by SIMS analyses. However, the analyzed images were taken only at the non-current flow condition. The effects of anodic polarization have not been clarified yet. Thus, in this paper, we report the effects of anodic polarization on the CH_4 decomposition and carbon deposition at the Ni-mesh/YSZ interfaces.

2. Experimental

2.1. Samples and isotope labeling experiments

Fig. 1 shows schematic diagram of isotope labeling experiments under voltage application (under anodic polarization). We have chosen nickel (Ni) as the test anode because Ni is a typical metal for porous anode material [8,9]. The Ni-mesh/YSZ samples were fabricated by the mechanical pressing of grid mesh. The bottom part of Fig. 1 shows the microstructure of the Ni-mesh/YSZ sample through the YSZ electrolyte. The thickness of the Ni-mesh was about 20 μm in this experiment. As an oxide substrate, a single crystal of Y_2O_3-stablized ZrO_2 (YSZ, 8 mol% Y_2O_3-doped) was applied. As shown in Fig. 1, the Ni-mesh/YSZ interface shows clear boundaries with no voids and cracks, suggesting a perfect contact between Ni-mesh and YSZ substrates.

A voltage was applied so that oxide ions (O^{2-}) were supplied to the Ni-mesh/YSZ interfaces. In this experiment, the voltage at the anode was set from 0 to 0.3 V versus a counter electrode (Pt). The current densities observed were from 0 to 20 mA cm^{-2}. Under anodic polarization, the isotope labeling was examined for the duration of 300 s, which corresponded to the following amount of oxygen conducted through the YSZ: 2×10^{-5} mol cm^{-2}. The amount of oxygen molecules is sufficient to cover the whole surface of Ni-mesh. Under this condition, atmospheric $^{18}O_2$ can conduct through the YSZ electrolyte and oxidize the deposited carbon on the Ni-mesh anode.

The current–voltage characteristic was measured under the mixtures of CH_4, D_2O, $^{18}O_2$, and Ar to simulate the steam reforming and direct-feeding of CH_4 into SOFCs. The total gas pressure was 0.35 bar, and the partial pressures of the mixed gases were in the following ratios: $p_{(CH_4)}/p_{(D_2O)}/p_{(^{18}O_2)} = 0.29/0.02/0.04$ bar. D_2O and $^{18}O_2$ were used to label the movements of hydrogen and oxygen, respectively. The thermodynamic equilibrium oxygen partial pressure is calculated to be around 10^{-23} bar, and the reformed gas composition is calculated

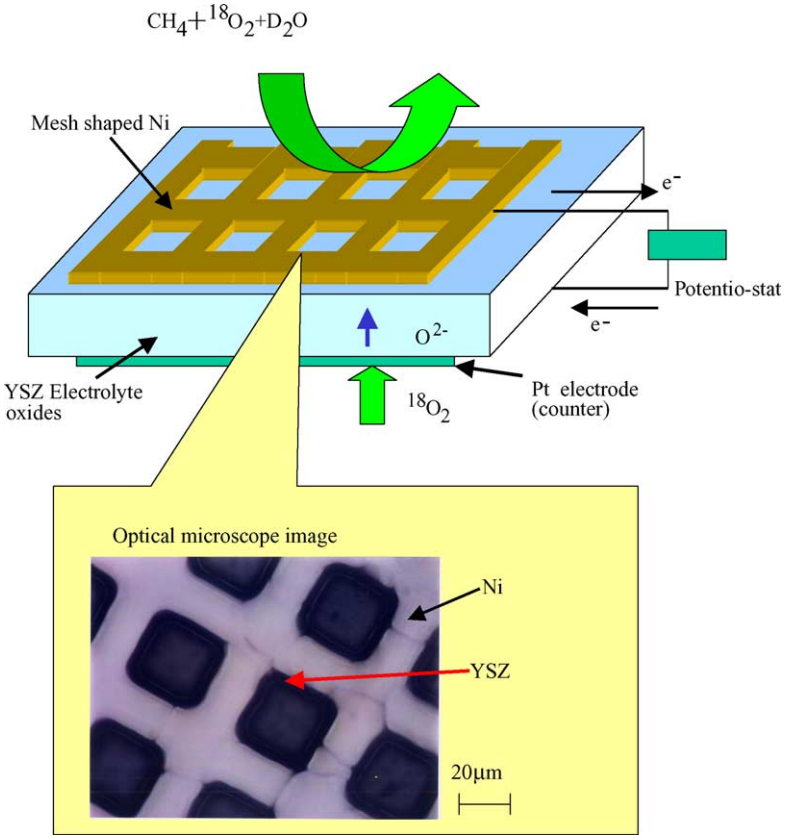

Fig. 1. Schematic diagram of isotope labeling experiment under voltage-applied condition.

from the thermodynamic calculation software as follows: $p_{(O_2)} = 2.23 \times 10^{-23}$ bar, $p_{(H_2)} = 5.80 \times 10^{-1}$ bar, $p_{(H_2O)} = 3.05 \times 10^{-3}$ bar, $p_{(CO)} = 7.61 \times 10^{-2}$ bar, $p_{(CO_2)} = 4.33 \times 10^{-4}$ bar, $p_{(CH_4)} = 8.64 \times 10^{-3}$ bar. At this oxygen partial pressure, carbon deposition does not occur when the equilibrium is attained. During the CH_4–H_2O treatments, the gas composition was checked with a mass monitor (RIGA-202, ULVAC Co.) by extracting small amounts of reaction gases: the measured $p_{(CO)}/p_{(CO_2)}$ ratio was about 100, which is of the expected similar order of magnitude. Thus, the gas mixture almost reaches equilibrium in this experimental condition.

2.2. SIMS analysis

After annealing in a CH_4–D_2O–$^{18}O_2$ atmosphere, the samples were quenched to room temperature within 30 s. This technique enables us to observe a "frozen state" of labeled elements distribution in the samples by secondary ion mass spectrometry (SIMS, CAMECA ims-5f, France) in its imaging mode. The primary ion beam was Cs^+ (accelera-

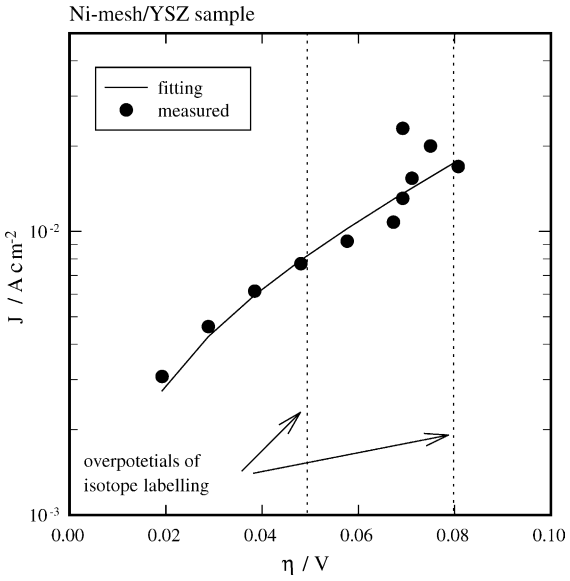

Fig. 2. Polarization curves of Ni-mesh/YSZ samples in $CH_4 + D_2O + {}^{18}O_2$ at 1073 K (solid line is fitting line for Butler–Volmer equation).

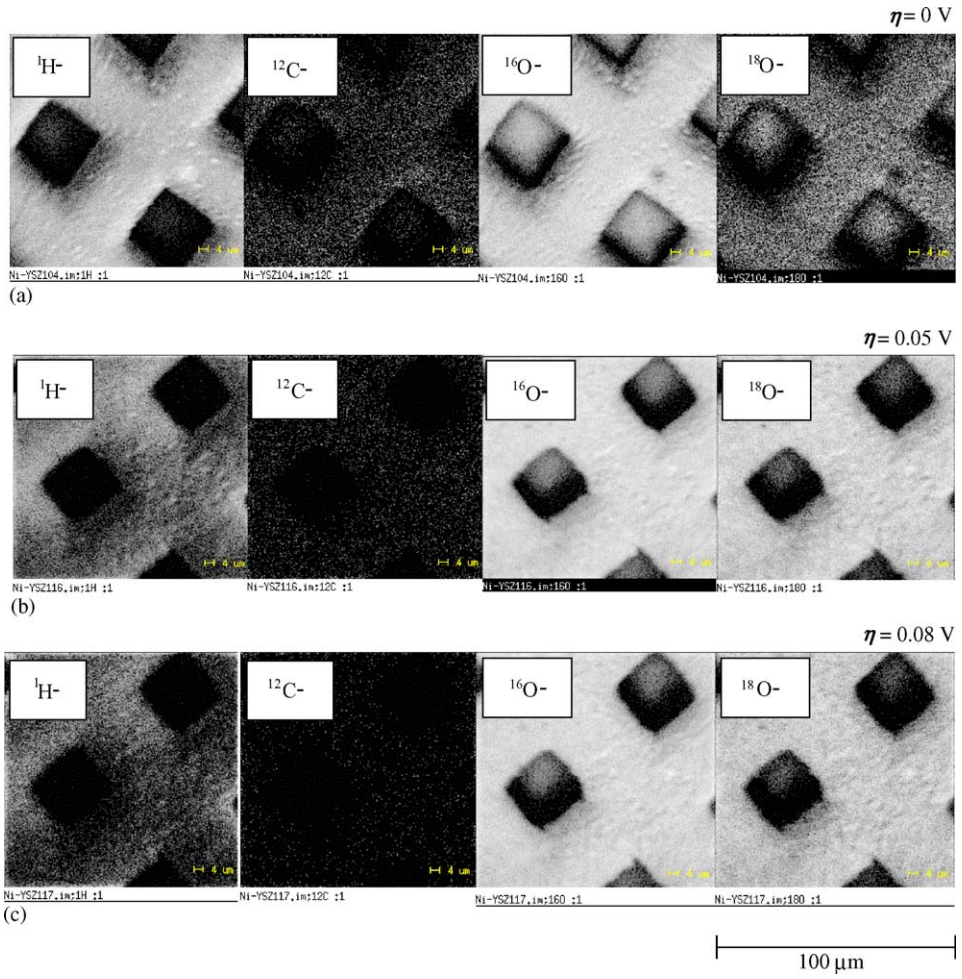

Fig. 3. Secondary ion mass spectrometry (SIMS) images for each element around the Ni-mesh/YSZ interfaces at different over-potentials: (a) $\eta = 0$ V, (b) $\eta = 0.05$ V and (c) $\eta = 0.08$ V.

tion voltage: 10 kV, primary beam current: less than 1 nA) and the distribution of negative secondary ions ($^2D^-$, $^{12}C^-$, $^{16}O^-$, $^{18}O^-$, $Ni^{16}O^-$, and $Zr^{16}O^-$) was measured in the area of 100 μm × 100 μm. After the SIMS analysis, the depths of the SIMS craters were measured by a surface profiler system (Dektak^3, Veeco/Sloan Technology, NY, USA).

3. Results and discussion

3.1. Polarization curves of the Ni-mesh/YSZ sample in CH_4–D_2O–$^{18}O_2$ atmospheres

Fig. 2 shows the polarization curve of the Ni-mesh/YSZ sample in the mixture of CH_4, D_2O, and $^{18}O_2$ at 1073 K. The over-potential (η) of the Ni-mesh/YSZ interface was estimated from the following equation assuming that the electrolyte resistance was constant:

$$\eta = E - JR_{(\text{electrolyte})} \tag{4}$$

where E is applied voltages between Ni-mesh and platinum counter electrode, J the current density through the electrolyte and $R_{(\text{electrolyte})}$ the resistance of the electrolyte (in this case, it was set as 10 Ω). The solid line in the figure shows the fitting lines of the Butler–Volmer equation to the measured data, as follows:

$$J = J^{\text{O}} \left[\exp(n\alpha_{\text{a}} f\eta) - \exp(-n\alpha_{\text{c}} f\eta)\right] \tag{5}$$

where J^{O} is exchange current density, n the number of electrons (in this case $n = 2$), α the transfer coefficient (in this case, $\alpha_{\text{a}} = \alpha_{\text{c}} = 0.5$), $f = F/RT$, ($F = 96{,}485\ \text{C mol}^{-1}$, $R = 8.314\ \text{J K}^{-1}\ \text{mol}^{-1}$, $T = 1073$ K), and η is over-potential defined above. From the fitting lines, the exchange current density (J^{O}) was calculated to be $3.2 \times 10^{-3}\ \text{A cm}^{-2}$, which was comparable to the reported values of Ni/YSZ cermet [8,9]. Thus, the mesh electrodes adopted in this study showed similar electrochemical properties to the porous Ni/YSZ cermet. The isotope labeling experiments were conducted at the two different over-potentials: 0.05 and 0.08 V. The current densities were high enough to supply oxygen to the Ni-mesh surface.

3.2. The effect of voltage application on the SIMS images of mesh-electrode/electrolyte interfaces

Fig. 3 shows SIMS images of Ni-mesh/YSZ interfaces at different voltage-applied conditions. The white parts indicate the higher concentration of each secondary ion. High concentration of $^1H^-$ is observed at the Ni parts for all the samples, whereas low concentration is observed at the YSZ parts. This indicates that the solubility of H and reactivity of H are high at the Ni-mesh. The concentration of $^2D^-$ is so low that we cannot observe the distribution clearly. The distribution of $^{12}C^-$ is somewhat different at the different applied voltages: high concentration of $^{12}C^-$ is observed on the Ni-mesh surface at $\eta = 0$ V, whereas the concentration is reduced at $\eta = 0.05$ V and $\eta = 0.08$ V. The images of $^{16}O^-$ indicate that high concentration parts are distributed both at the Ni-mesh surface and the YSZ surface, suggesting a similar catalytic activity for the oxygen reaction. At the voltage-applied condition, the $^{18}O^-$ images show the higher concentration at the Ni-mesh parts, suggesting that high amounts of ^{18}O were supplied from the gas phase from the Pt-counter electrode to the Ni-mesh surface.

To analyze each elemental distribution quantitatively, line analysis has been applied in these images. Fig. 4 shows line analyses of each secondary ion. The ^{18}O concentration, $C_{^{18}\text{O}}(x)$, was defined as the ratio of SIMS signals of $^{16}O^-$ and $^{18}O^-$ in the following:

$$C_{^{18}\text{O}}(x) = \frac{I_{^{18}\text{O}}(x)}{I_{^{18}\text{O}}(x) + I_{^{16}\text{O}}(x)} \tag{6}$$

where, $I_{^{18}\text{O}}(x)$ and $I_{^{16}\text{O}}(x)$ indicate SIMS signal intensities of $^{16}O^-$ and $^{18}O^-$ at a lateral position of x, respectively. In Fig. 4a, the ^{18}O concentration is plotted as a function of the lateral position. Under the zero-voltage-applied condition ($\eta = 0$ V), the ^{18}O concentration at the Ni-mesh shows a low value compared with the YSZ parts. On the other hand, under the voltage-applied condition ($\eta = 0.05$ and 0.08 V), the ^{18}O concentration at the Ni-mesh shows relatively high values. This indicates that the atmospheric $^{18}O_2$ can be transported from the counter electrode to the

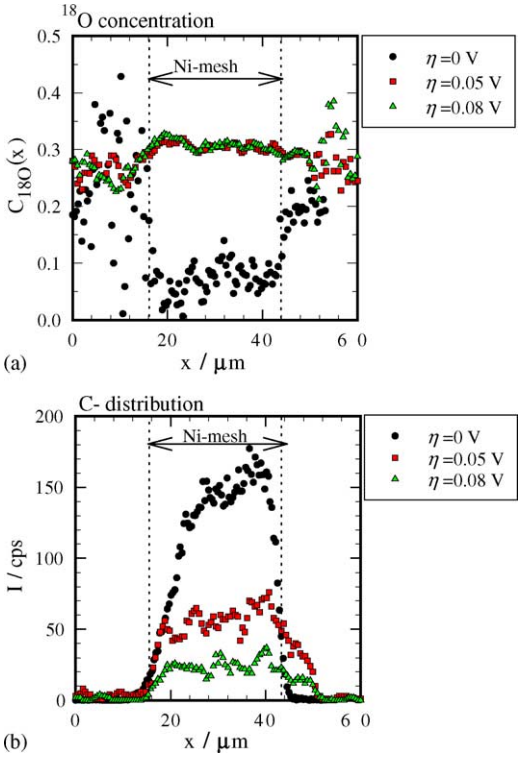

Fig. 4. Line analyses of SIMS images around the Ni-mesh/YSZ interfaces at different over-potentials: (a) line analyses of ^{18}O concentration and (b) line analyses of carbon.

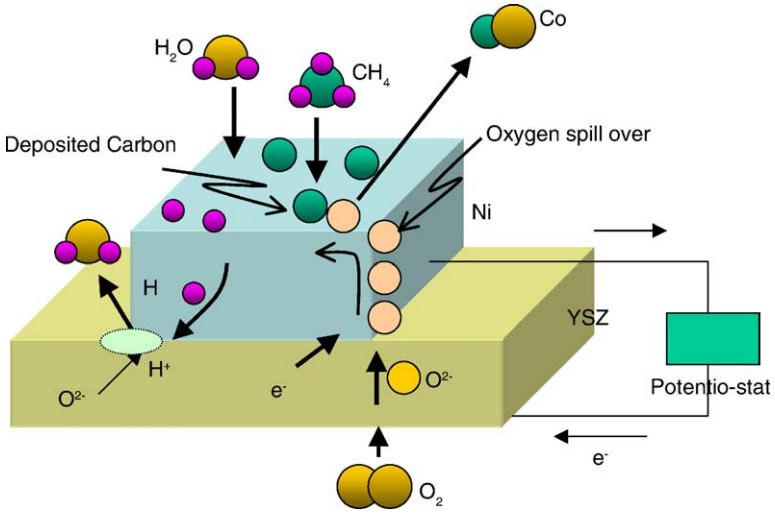

Fig. 5. Models of CH_4 decomposition and elimination of carbon deposition by the applied voltage.

Ni-mesh surface through the YSZ electrolyte. The signal intensity of $^{12}C^-$ shows a clear difference between the zero-voltage and the voltage-applied conditions (Fig. 4b): the signal intensity of $^{12}C^-$ is decreased with increasing over-potentials. Thus, the amount of deposited carbon on the Ni-mesh surface is decreased significantly by the voltage application. This suggests that the oxygen supplied to the Ni-mesh surface effectively oxidizes the deposited carbon. The oxygen spill-over from the Ni/YSZ interface can effectively oxidize the deposited carbon on the Ni-mesh surface.

3.3. Models of carbon elimination and direct oxidation of CH_4 around the metal–oxide interfaces

From the SIMS images and line analyses, the Ni surface is active for CH_4 decomposition compared with YSZ surface. Thus, Ni metal is indispensable CH_4 decomposition and not only for current collectors. Fig. 5 shows a schematic diagram of CH_4 decomposition and elimination/oxidation of deposited carbon around the Ni/YSZ interfaces. The Ni surface should be active for CH_4 decomposition and reaction with the reformed gases (such as H_2 and CO). Under zero-voltage application ($\eta = 0$ V), CH_4 decomposition and carbon deposition occurs on the Ni surface. On the other hand, under the voltage application, the oxide ions (O^{2-}) conducted through the YSZ electrolyte can spill over from the Ni/YSZ interface to the Ni surface (under fuel cell operation conditions). Therefore, the supplied oxygen can effectively oxidize the deposited carbon on the Ni surface (thickness 20 μm). The amounts of oxygen molecules supplied by the voltage application were enough to cover the whole surface of Ni-mesh in this experimental condition. When the amounts of oxide ion supplied are appropriately controlled, the deposited carbon can be eliminated on the Ni surface. In practical porous Ni-oxide cermets, the control of Ni size and distribution will be most important.

4. Conclusion

By SIMS imaging analysis, the effect of applied voltages on surface catalytic activities was compared at the Ni-mesh/YSZ interfaces for CH_4 decomposition and elimination of carbon deposition. A labeling experiment was examined in the mixture of CH_4, D_2O, and $^{18}O_2$ at 1073 K. A significant carbon deposition was observed at the Ni-mesh. However, the applied voltages can eliminate the deposited carbon on the Ni-mesh effectively. The control of the oxygen spill-over from the Ni/YSZ interface can be important for designing the optimum interface structure. A possible reaction mechanism was considered for the optimum metal–oxide interface of SOFCs.

Acknowledgements

Part of this study was supported by the Industrial Technology Research Grant Program in 2002–2004 from New Energy and Industrial Technology Development Organization (NEDO) of Japan. The corresponding author is grateful to the organization.

References

[1] R.M. Ormerod, High temperature solid oxide fuel cells: fundamentals and applications, in: S.C. Singhal, K. Kendall (Eds.), Fuels and Fuel Processing, Elsevier, Chapter 12, 2003.
[2] H. Kim, S. Park, J.M. Vohs, R.J. Gorte, J. Electrochem. Soc. 148 (7) (2001) A693.

[3] H. Kim, C. Lu, W.L. Worrel, J.M. Vohs, R.J. Gorte, J. Electrochem. Soc. 149 (3) (2002) A247.
[4] O.A. Marina, C. Bagger, S. Primdahl, M. Mogensen, Solid State Ionics 123 (1999) 199.
[5] H. Uchida, S. Suzuki, M. Watanabe, Solid Oxide Fuel Cells VIII, PV2003-17, The Electrochemical Society Inc., NJ, pp. 728.
[6] T. Horita, K. Yamaji, T. Kato, N. Sakai, H. Yokokawa, J. Power Sources 131 (2004) 299.
[7] T. Horita, K. Yamaji, T. Kato, N. Sakai, H. Yokokawa, Solid State Ionics 169 (2004) 105.
[8] H. Itoh, T. Yamamoto, M. Mori, T. Horita, N. Sakai, H. Yokokawa, M. Dokiya, J. Electrochem. Soc. 144 (1997) 641.
[9] Y. Jiang, A.V. Virkar, J. Electrochem. Soc. 148 (7) (2001) A706.